(Received 14 December 2025, Accepted 6 January 2026, Scheduled 16 February 2026)

Anisotropic Modelling of the Electromagnetic Response of 3D-Printed Carbon Nanotube/Polymer Nanocomposites for Shielding Applications

Ailar Sedghara[1,2], Ehsan Khoshbakhti[2], Hadi Hosseini[2], Mohammad Arjmand[2,*], and Loïc Markley[1,*]

[1]*Applied Electromagnetics Laboratory, School of Engineering, Faculty of Applied Science University of British Columbia, Kelowna, BC V1V 1V7, Canada*
[2]*Nanomaterials and Polymer Nanocomposites Laboratory (NPNL), School of Engineering Faculty of Applied Science, University of British Columbia, Kelowna, BC V1V 1V7, Canada*

ABSTRACT: This study explores the anisotropic electromagnetic properties of carbon nanotube (CNT)/polylactic acid (PLA) nanocomposites, fabricated in-house and shaped using traditional compression molding and advanced 3D printing techniques. By examining the effects of CNT content (ranging over 1–4 wt.% (weight percent)) and 3D printing path orientation, this research investigates how these factors influence shielding effectiveness (SE) and the corresponding nanocomposite complex dielectric permittivity tensor. Notably, a significant variation in SE was observed between the different printing path orientations, with a difference of over 20 dB at 4 wt.% CNT. Experimental measurements were used to develop an anisotropic model for the complex dielectric permittivity, with the permittivity components for samples at 4 wt.% CNT extracted to be $36.5 - j44.5$ along the printing direction ($\varepsilon_{\parallel}$) and $8.3 - j3.1$ in the perpendicular direction ($\varepsilon_{\perp}$) over the X-band frequency range (8.2–12.4 GHz). These findings demonstrate that CNT alignment during 3D printing induces highly directional electromagnetic properties. Furthermore, we demonstrate that anisotropic simulation models provide a more accurate prediction of the electromagnetic response of 3D-printed nanocomposite structures than isotropic models. In brief, this study emphasizes the necessity of considering anisotropic properties in the design and simulation of 3D-printed nanocomposites for electromagnetic shielding and other applications.

1. INTRODUCTION

Electromagnetic interference (EMI) can disrupt critical systems in sectors such as aerospace, defense, and telecommunications [1]. Concerns regarding these disruptions have increased with the proliferation of electronic devices and wireless functionality. Traditional EMI shields are typically made of metal, offering effective protection but with notable drawbacks, such as weight, rigidity, and susceptibility to corrosion. Conductive polymer nanocomposites, particularly those incorporating conductive nanoparticles such as carbon nanotubes (CNTs), address these issues by offering lightweight, flexible, and corrosion-resistant alternatives [2]. Polylactic acid (PLA) is a renewable and biodegradable polymer that is electrically insulating, has a high tensile strength relative to other biodegradable polymers, and is compatible with 3D printing technology [3]. Incorporating CNTs into PLA increases its electrical conductivity, making it suitable for EMI shielding, while also increasing its thermal conductivity and reducing brittleness [4].

The complex dielectric permittivity of nanocomposites plays a critical role in their EMI shielding performance by directly influencing how these materials interact with, absorb, reflect, and attenuate electromagnetic waves across various frequency ranges. Accurate permittivity measurements are vital for optimizing the EMI shielding performance of materials. Many studies have explored the permittivity of pure PLA over a wide frequency range [5–8]. However, discrepancies exist in the reported permittivity values even at the same frequencies, likely due to differences in the measurement and extraction methods used in these studies. For CNT/PLA nanocomposites, only a limited number of studies have reported the permittivity values. For instance, Bertašius et al. [9] and Beltrán et al. [10] provided permittivity data for the frequency range of 26–40 GHz. However, the reported values vary significantly across these studies, with discrepancies of up to 60% in the real part of permittivity within the same frequency range. The variation in the reported values of CNT/PLA nanocomposites in the literature demonstrates the need for consistent, reliable, and effective parameter extraction methods, which are essential for the accurate design of EMI shielding structures.

The distribution and alignment of CNTs within a matrix have been shown to induce anisotropic electrical responses [11]. Therefore, understanding these anisotropic properties is crucial for accurately predicting the EMI shielding performance of nanocomposite materials. Various methods have been employed to induce alignment of nanofillers. They include the use of shear-induced alignment, which is injection molding [12], and the use of electric, magnetic, or acoustic fields [13–15]. However, these methods often have limitations, including

* Corresponding authors: Loïc Markley (loic.markley@ubc.ca); Mohammad Arjmand (mohammad.arjmand@ubc.ca).

complex setup requirements, challenges in achieving precise nanofiller alignment, and scalability issues. Additionally, maintaining uniform alignment over large areas can be difficult, and the process may become costly or inefficient for mass production [16].

Recently, 3D printing has gained significant attention for its ability to create complex shapes at high speeds and for applications in industries such as aerospace and medicine [17, 18]. Various 3D printing techniques, including fused deposition modelling (FDM), selective laser sintering (SLS), and stereolithography (SLA), allow the production of prototypes and models with reduced wastage and operational costs. Among these methods, FDM is particularly popular owing to its affordability and simplicity, making it a widely used technique for producing high-strength and lightweight parts across various sectors.

Some recent studies have demonstrated that 3D printing can induce anisotropy in composites; however, these studies either concentrated on resistivity and SE measurements or considered carbon fiber inclusions rather than carbon nanotubes (whose dimensions are several orders of magnitude smaller). While some studies report permittivity measurements, a significant gap remains in the development of anisotropic models that effectively link material configuration to high-frequency electromagnetic behavior, restricting their application in complex design implementations. For instance, Zohdi and Yang [19] reviewed additive manufacturing (AM) as a versatile technology capable of fabricating complex-shaped products with mechanical, thermal, and electrical properties that can exhibit anisotropic behavior. Truman et al. [20] investigated 3D-printed PLA composites filled with carbon black and demonstrated that the electrical resistivity strongly depends on the printing infill pattern and filament orientation, and Wu et al. [21] proposed 3D-printed polycaprolactone composites filled with carbon nanofibers to evaluate their EMI shielding performance, noting their strong orientation-dependent DC electrical conductivities. Another work by Harmon et al. [22, 23] investigated colorFabb XT-CF20, a carbon-fiber-loaded filament, and demonstrated that the anisotropy of the real part of the permittivity could be represented by a diagonal tensor with elements equal to 41.1, 4.6, and 6.4 at a frequency of 100 kHz. They concluded that anisotropy arises from the alignment of carbon fiber inclusions along the 3D printing path. Their measurements were restricted to frequencies below 300 MHz and did not present an anisotropic analysis of the imaginary permittivity component. Similarly, Mahaut et al. [24] evaluated the EMI shielding effectiveness (SE) of carbon-fiber-reinforced nylon nanocomposites in the X-band frequency range. They investigated the effect of anisotropy on SE by varying the fiber alignment. However, anisotropic parameter models were not proposed. Another study by Compton and Lewis [25] used 3D printing to align SiC and carbon fibers in layered nanocomposites to investigate the anisotropic properties of the hexagonal macrostructure. However, the anisotropic properties of the microstructures were not explored.

Here, we explore the anisotropic electromagnetic properties of CNT/PLA nanocomposites fabricated using compression molding and FDM 3D printing techniques. The use of 3D-printed samples allowed for detailed characterization of the anisotropic properties of these nanocomposites. We present anisotropic models of complex permittivity for samples with varying CNT content and orientation. These models highlight the importance of considering the alignment of 3D printing paths in the design of EMI shielding structures. Moreover, these methods provide precise models necessary for designing other 3D-printed structures made from these materials.

2. MATERIALS AND SAMPLE PREPARATION

PLA was purchased from Filabot (Luminy LX175), and multi-walled carbon nanotubes were purchased from Nanocyl (NC7000 TM series). These nanotubes, produced via the Catalytic Chemical Vapor Deposition (CCVD) process, have an average diameter of 9.5 nm and an average length of 1.5 µm, according to the manufacturer's specifications, as measured by transmission electron microscopy. PLA pellets and CNT powder were melt-blended using a pilot-scale twin-screw extruder (HAAKE^{TM} Rheomex CTW100 OS) equipped with four different temperature zones set to 170°C in zone 1 (feeding), 175°C in zone 2 (melting), 175°C in zone 3 (metering), and 180°C in zone 4 (die). A 2 mm rod-shaped die was attached to the extruder to produce polymer nanocomposite filaments with a diameter of 1.75 mm. The screw speed was set to 20 rpm. The extruded filaments were cooled in a water bath at room temperature before being wound onto the spools using a spooler. The filament diameter was controlled by adjusting the spooler rotational speed. To prepare CNT/PLA nanocomposite filaments, CNTs were blended with PLA at CNT loadings of 1%, 2%, 3%, and 4% by weight. After filament fabrication, the samples were produced using two different methods, compression molding and FDM 3D printing, as shown in Figure 1. All the samples were molded or cut to match the dimensions of a WR-90 waveguide (22.86 mm × 10.16 mm), which is a standard size used in microwave and RF testing. Ensuring precise mold dimensions is crucial for eliminating potential measurement errors caused by air gaps between the sample and waveguide walls. These accurate measurements are essential for obtaining reliable data on electromagnetic properties, including the complex dielectric permittivity and shielding effectiveness.

Compression molding was carried out using a Carver Bench Top Manual ASTM Press at 190°C under 20,000 psi pressure for 5 min, followed by quenching with water before sample removal. This process produced samples with randomly oriented and uniformly distributed CNTs, as reported for compression-molded CNT composites [12]. A Raise 3D Pro2 Plus 3D printer and IdeaMaker 4.3.3.6 software were employed for FDM 3D printing to fabricate samples with different path orientations. Nanocomposite filaments prepared using the extrusion process were used for 3D printing. The printer featured a 0.4 mm nozzle diameter, with the nozzle and bed temperatures set to 190°C and 60°C, respectively. The printing speed was set to 30 mm/s.

To ensure the precise characterization of the anisotropic response of 3D-printed nanocomposites, larger samples were fabricated, carefully cut, and sanded to remove any paths that were not aligned with the target path orientation. The 3D printer

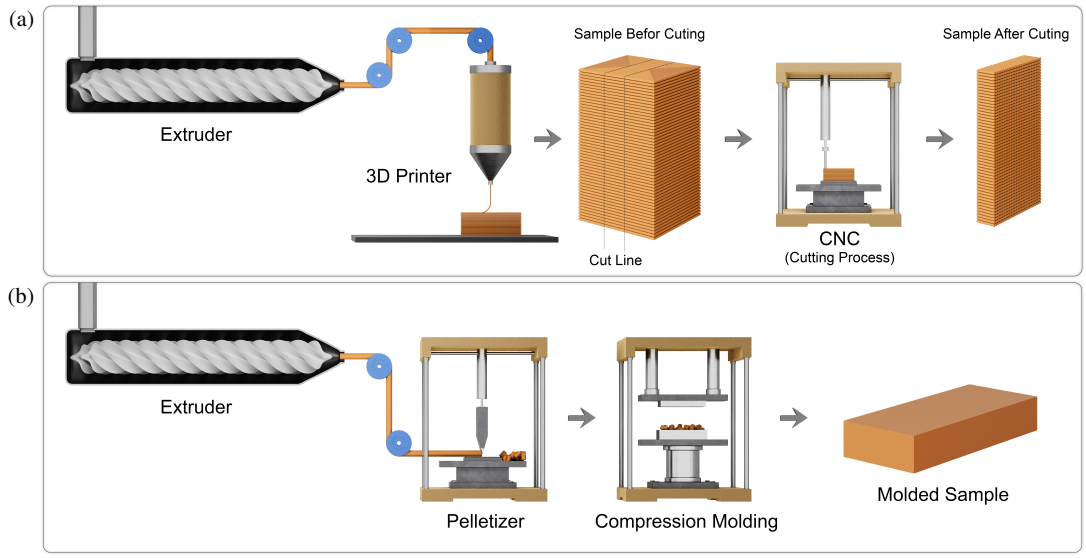

FIGURE 1. Schematic representations of two sample fabrication processes: (a) extruded CNT/PLA filaments are converted into pellets, which are then placed into a compression mold to produce samples with randomly aligned CNTs; (b) extruded CNT/PLA filaments are fed into an FDM 3D printer to fabricate blocks that are cut with a CNC to obtain samples with uniformly aligned printing paths and hence uniformly aligned CNTs.

was programmed to print samples using a concentric square spiral path. By increasing the sample dimensions, an interior region with uniformly oriented paths is formed. As illustrated in Figure 2, cutting lines were chosen to isolate the sections of the printed blocks corresponding to each principal direction. The samples were cut using a UMC-750 Computer Numerical Control (CNC) machining center. The edges of each sample were smoothly finished using 1500-grit sandpaper. The samples were labeled according to their 3D printing path orientation. For example, the X-print samples were printed with the printing paths aligned parallel to the x-axis of the waveguide. This preparation method resulted in samples with uniform anisotropy, enabling accurate characterization of the sample properties for different printing orientations.

3. EXPERIMENTAL RESULTS

3.1. Anisotropic Electric and Electromagnetic Characterizations

The shielding effectiveness quantifies the ability of a structure to block the transmission of EM waves. It is influenced by factors such as frequency, shield material, and shield geometry. The SE, initially introduced by Schelkunoff [26], is the power ratio of the incident wave to the transmitted wave and is expressed in dB. This is mathematically represented by Equation (1):

$$\mathrm{SE} = 10\log_{10}\left(\frac{P_I}{P_T}\right) = 10\log_{10}\left(\frac{1}{|S_{21}|^2}\right) \tag{1}$$

where P_I is the incident power, P_T is the transmitted power, and S_{21} is the transmission coefficient, respectively.

The EMI shielding performance was measured by placing the samples in a WR-90 rectangular waveguide and using a Keysight P9374A vector network analyzer (VNA) to measure the complex scattering parameters (S-parameters) over the X-band frequency range (8.2–12.4 GHz). The measurements were calibrated using a WR-90 waveguide calibration kit (through-reflect-line) with the samples placed inside a quarter-wavelength waveguide section, and the measured S-parameters were de-embedded onto the surface of the sample. The sample was electrically centered within the waveguide through this de-embedding process by matching the phase responses of S_{11} and S_{22}.

Figure 3 presents a comparison of the SE over the X-band frequency range between CNT/PLA nanocomposite samples fabricated via compression molding and those fabricated using a 3D printer, with printing paths oriented along each of the coordinate axes. Comparisons were performed for the samples with four CNT content levels. As expected, we observed an increase in the SE of the molded samples with increasing CNT content (purple traces). We also observed a significant difference in the SE of the 3D-printed samples based on the path orientation. The strongest response was observed for the Z-print samples, where the printing paths were aligned with the waveguide electric field. These samples produced an SE that was within 1.1–4.6 dB of that of the molded samples. In contrast, the X-print and Y-print samples, in which the printing paths were perpendicular to the waveguide electric field, produced a much lower SE. Specifically, the X-print and Y-print SE values were always at least 4.3 dB, 12.4 dB, 20.6 dB, and 21.9 dB below the Z-print SE for the 1, 2, 3, and 4 wt.% samples, respectively.

The electrical conductivities of the three 3D-printed samples and a molded reference sample were measured using a Loresta GX four-probe resistivity meter (MCP-T700 model, Mitsubishi Chemical Co., Japan). The results are shown in Figure 4. All samples had identical dimensions and were positioned with their longer dimensions and the largest face aligned under the

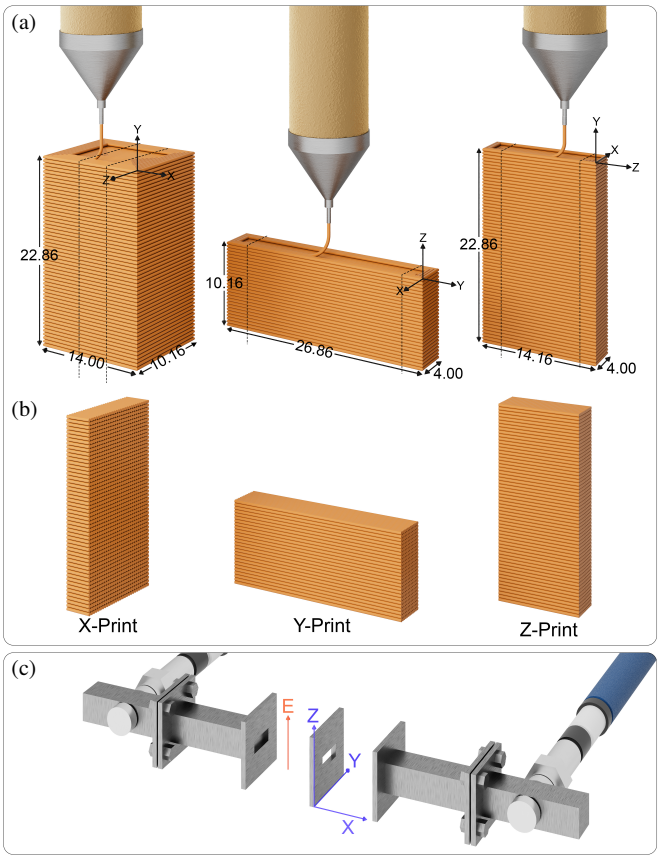

FIGURE 2. An illustration depicting the fabrication and testing process of 3D-printed samples. The samples are labeled as X-Print, Y-Print, or Z-Print, based on the orientation of the 3D printing paths relative to the waveguide test set axes. (a) The raw 3D-printed samples are shown with dimensions (in mm) and dashed cutting lines. (b) Final printed samples after the excess material is removed, and all printing paths are aligned. These samples all have a cross-section that matches the WR-90 waveguide cross-section (22.86 mm × 10.16 mm) and have a thickness of 4 mm. (c) The waveguide test set with a reference coordinate axis and a red arrow representing the electric field polarization.

four-point probe, as illustrated in the inset. The molded sample was included for comparison, showing higher conductivity across all CNT concentrations. Its conductivity increased smoothly, suggesting that percolation (i.e., the formation of a continuous, interconnected network) occurs below 1 wt.% CNT. In contrast, the 3D-printed samples exhibited a sharp increase in conductivity when the CNT content exceeds approximately 2 wt.%, indicating the onset of a percolation threshold and the formation of conductive networks within the PLA matrix. The conductivity values for the Y-print and Z-print samples, with printing paths aligned along the surface, were nearly identical. In contrast, significant differences were observed for the X-print samples, whose printing path was perpendicular to the surface, supporting the anisotropic behavior of the material. Although four-point probe measurements can differentiate between in-plane and out-of-plane conductivities, they cannot resolve in-plane anisotropy (that is, in-plane conductivity along vs. across the printing path), as noted in previous studies [27].

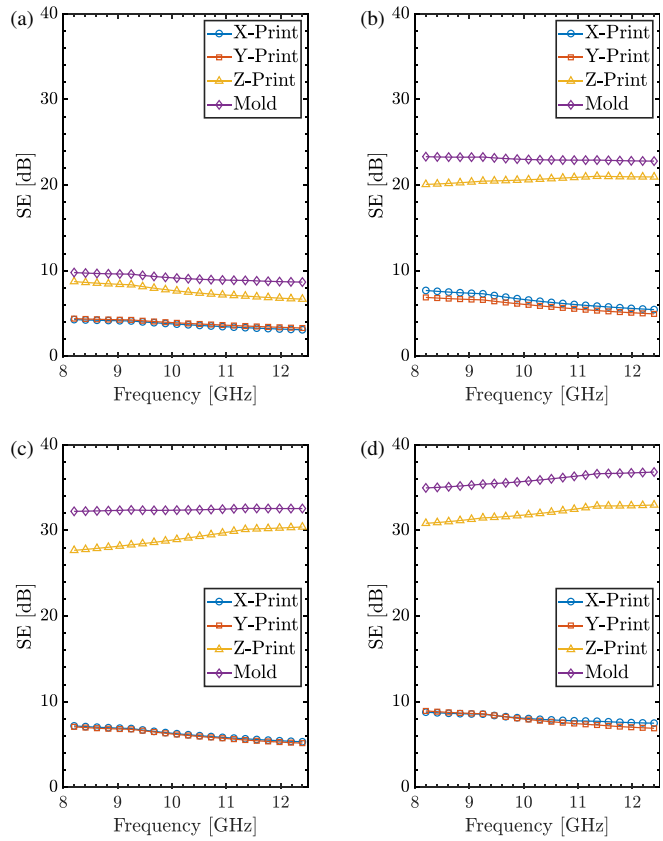

FIGURE 3. EMI shielding effectiveness over frequency for printed samples with three different path orientations and for compression-molded samples. Samples were formed from nanocomposite material with CNT content at four different weight percentages: (a) PLA-1% CNT, (b) PLA-2% CNT, (c) PLA-3% CNT, (d) PLA-4% CNT.

3.2. Micro-Structural Characterization

To gain further insight into the alignment of CNTs during the FDM 3D-printing process, we used rheological measurements to compare the physical properties of compression-molded samples to their 3D-printed counterparts. Rheology studies the flow and deformation of materials under applied stress forces, which provides information about the micro-structures of different materials [28], and in the case of polymer-CNT nanocomposites, it can infer information about the 3D structure of the CNT network. To conduct this investigation, samples formed from pure PLA and from CNT-PLA nanocomposite material were analyzed using an Anton Paar Rheometer MCR 102 in parallel plate geometry with a plate diameter of 25 mm. The measurements were performed at 180°C under a nitrogen atmosphere to prevent thermal degradation, with a gap of 1 mm. Steady shear (flow) tests were performed over a low shear rate range of 0.08 to 3 s^{-1} to investigate the nonlinear rheological behavior of the samples.

From a rheological perspective, flow curves at low shear rates, where the CNT network has not yet been disrupted, can provide valuable insights into the alignment of CNTs. Because the rheological measurement process is destructive, we fabricated two different 3D-printed samples with printing paths aligned parallel to the rheometer plates (labeled Print 1 and Print 2) and compared them with a molded sample.

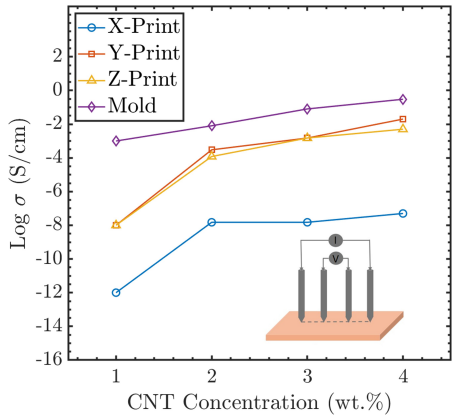

FIGURE 4. Electrical conductivity vs. CNT content of the nanocomposites measured for each of the 3D-printing samples. Conductivity was assessed using a four-point probe aligned with the longer dimension of each sample, as illustrated in the inset. Note that in the X-Print sample, the 3D-printing paths were aligned perpendicular to the surface, while in the Y-Print and Z-Print samples, they were aligned parallel to the surface.

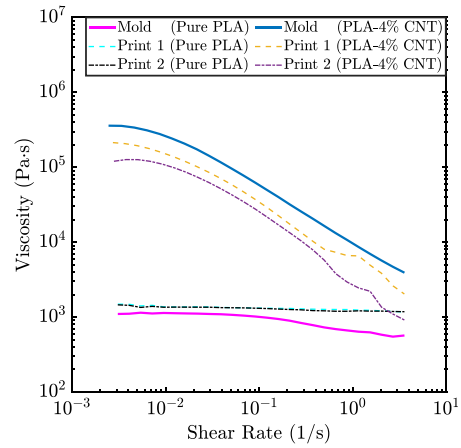

FIGURE 5. Flow curves showing viscosity as a function of shear rate for pure PLA, and PLA-4%CNT samples prepared via compression molding and 3D printing. Two 3D-printed samples were made, labeled as Print 1 and Print 2.

Figure 5 plots the viscosity of different samples as a function of shear rate. Firstly, in the case of pure PLA, we see that 3D-printed samples exhibit a near-zero-shear-rate viscosity that is 1.3 times larger than for compression molded samples, with measured values of 1455 Pa·s and 1100 Pa·s, respectively. This would be possibly attributed to the higher crystallinity of the aligned PLA macromolecule chains under 3D printing [29, 30]. However, the presence of CNTs and their distribution within the PLA matrix significantly influenced the flow curves. As observed in the flow curves of the nanocomposite counterparts, the presence of CNTs increased the low-shear-rate viscosity by two orders of magnitude, and a clear "shear-thinning" behavior was detected, where the viscosity decreased with increasing shear rate. Furthermore, in contrast to the pure PLA case, the 3D-printed nanocomposite samples exhibited significantly lower viscosity than the compression-molded sample. Specifically, Print 1 shows a zero-shear viscosity of 2.5×10^5 Pa·s), which is approximately 1.7 times lower than that of the molded sample (4.2×10^5 Pa·s). Print 2 exhibits an even lower viscosity of (1.4×10^5 Pa·s), making it 3.0 times lower than its molded counterpart.

The reduced viscosity in CNT-PLA samples that were 3D printed suggests increased CNT alignment owing to the shear forces imparted during the printing process. While shear-induced orientation of PLA chains may occur during 3D printing, its contribution to dielectric anisotropy is marginal relative to the dominant role of CNT alignment in the investigated frequency range. These outcomes are consistent with the understanding that randomly percolated systems (i.e., systems where CNTs are randomly distributed in 3D space to form a continuous, interconnected network) should have higher viscosity than those with aligned CNTs. When CNTs are randomly dispersed, they form a more extensive and interconnected network throughout the polymer, which creates more entanglements and physical interactions between the polymer and CNTs, thereby increasing the resistance to flow. The CNT network significantly restricts the movement of the polymer chains, resulting in a higher viscosity. In contrast, in systems where the CNTs are aligned, they do not form 3D network structures, reducing the number of CNT-CNT and CNT-polymer interactions in the transverse direction. This decreases the restriction on polymer chain mobility, resulting in a lower viscosity. A similar observation was reported for polycarbonate/CNT nanocomposites prepared via compression molding compared with injection molding methods [31]. We can conclude from this investigation that the 3D-printing process disrupts the CNT network by aligning the CNTs in the direction of the 3D printing paths. This confirms the anisotropic micro-structure, which provides a mechanism for anisotropy observed in the electric and electromagnetic characterizations.

4. ANISOTROPIC PARAMETER EXTRACTION

4.1. Macro-Structural Electromagnetic Simulations

The variation in EMI shielding effectiveness relative to the printing path direction was observed by Verma et al. [32], who studied a polypropylene random copolymer (PPR) reinforced with multi-walled carbon nanotubes. They hypothesized that this variation arose from the internal voids between the FDM printing paths. To test this hypothesis, we compared the full-wave simulations in Ansys High-Frequency Structure Simulator (HFSS) of the shielding effectiveness of solid samples against two sets of perforated samples containing 0.4 mm diameter cylindrical air voids. The nanocomposite material was modeled using isotropic complex permittivity (non-magnetic) to isolate the effect of voids on the SE. A permittivity of $35 - j45$ over the X-band was used as a representative material parameter because it provided an SE similar to that observed in the experiment.

The voids were arranged in a square lattice with a periodicity of 0.8 mm, with one sample (Z-Print) having the voids aligned with the electric field and the other sample (Y-Print) having the voids aligned perpendicular to the electric field. The solid sample represents compression-molded samples (Mold).

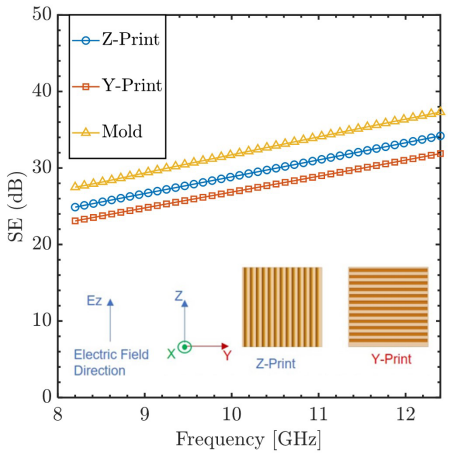

FIGURE 6. Simulated shielding effectiveness (SE) as a function of frequency for Z-Print, Y-Print, and compression-molded samples. The inset illustrations show Z-Print and Y-Print structures with cylindrical air inclusions. The electric field direction is also indicated for reference.

The SE was simulated for normal plane-wave incidence using wave port excitations in HFSS and perfect electric and magnetic boundary conditions. The thickness of the sample was set to 4.0 mm. As shown in Figure 6, the simulation results indicate that while the air voids do affect the SE, they cannot explain the difference of more than 20 dB observed between the 3D-printed samples with different printing path orientations. The maximum difference in SE between the Z-print and Y-print samples for the isotropic samples with air voids was 2.3 dB. Note that the drop in SE with respect to the solid (unperforated) samples can be explained by the 80.4% material fill factor arising from air voids.

Because the anisotropy of the 3D-printed samples cannot be explained solely by the air-void model, the CNTs within the PLA matrix must exhibit an anisotropic response resulting from the 3D printing process. Specifically, shear flow and viscous flow are the primary and secondary factors, respectively, that influence the alignment of CNTs within the nozzle during extrusion. This CNT alignment plays a critical role in determining the properties of 3D-printed samples. In the next section, we model the anisotropy using a permittivity tensor and demonstrate how tensor elements corresponding to directions parallel and perpendicular to the 3D printing paths can exhibit significantly different values.

4.2. Extraction of Anisotropic Electric Material Properties

The Nicolson-Ross-Weir (NRW) method [33, 34] was employed to extract the complex permittivities of the PLA and CNT/PLA nanocomposite samples. To apply the NRW method to scattering parameter measurements taken from a waveguide test-set, we used the waveguide mode impedance and waveguide mode propagation constant (for the TE_{10} mode) in the extraction [35]. Because the NRW extraction method is known to produce multiple solutions corresponding to different order resonances within samples, the correct solution branch was determined by comparing the extracted material parameters from samples of different thicknesses. We also prepared thin samples with thicknesses of 0.5 mm and 1 mm to provide reference solutions with widely spaced branches, which simplified the process of selecting the branch for the 4 mm samples. The correct branch choice was further confirmed by observing that the extracted permeability exhibited a non-magnetic response, consistent with the expected behavior of a nanocomposite material with conductive but non-magnetic fillers.

Let us now consider the complex permittivity of compression-molded samples placed in a waveguide test environment. Because the CNTs are randomly oriented within the PLA matrix in compression-molded samples, we can expect the electrical properties to be isotropic [12]. Therefore, we can employ the NRW method to extract the real and imaginary parts of permittivity. These data are plotted in Figure 7 for the X-band. We can observe that both the real and imaginary components of the permittivity increase as the CNT content increases within the PLA matrix. The increase in real permittivity can be attributed to the formation of a denser CNT population, which enhances the effective dielectric response by increasing the capacitance between neighboring CNTs as well as the capacitance within CNTs owing to defects and functional groups [36]. In the X-band frequency range, this effect dominates other polarization mechanisms, as both dipolar polarization (which typically occurs in polar materials up to the GHz range) and interfacial polarization (Maxwell-Wagner-Sillars effect [37, 38], with its long relaxation times) being negligible at these frequencies.

The imaginary component of permittivity also increases owing to the formation of conductive networks within the PLA matrix [39]. Over the X-band, both the real and imaginary permittivity components showed a relatively flat frequency dependence. These data show that we can design our nanocomposite to exhibit complex permittivities that range from approximately $3.0 - j0.01$ (pure PLA) to $34.3 - j55.4$ (4 wt.%) and beyond. The availability of these permittivities offers precise control over the properties of the materials used in the design of electromagnetic structures, particularly those intended for shielding applications.

Now, let us consider the 3D-printed samples with different printing path orientations. As demonstrated in Section 4.1, the SE was strongly influenced by these orientations, primarily because of the preferred alignment of CNTs along the printing path direction. We will now explore how the path orientation affects the anisotropy of the complex permittivity. We modeled the permittivity and permeability of the 3D-printed CNT/PLA nanocomposite using uniaxial diagonal tensors with components that were either aligned with the CNTs (i.e., $\varepsilon_{\parallel}$ for permittivity and $\mu_{\parallel}$ for permeability) or perpendicular to the CNTs (i.e., $\varepsilon_{\perp}$ and $\mu_{\perp}$).

Although experimental observations drive this modelling, they are also supported by theoretical frameworks. Classical effective medium theories, including the Clausius-Mossotti and Maxwell-Garnett models, have been extended in prior studies to account for anisotropic inclusions, such as aligned CNTs. These approaches incorporate depolarization factors or orientation distribution functions to reflect the directional dependence

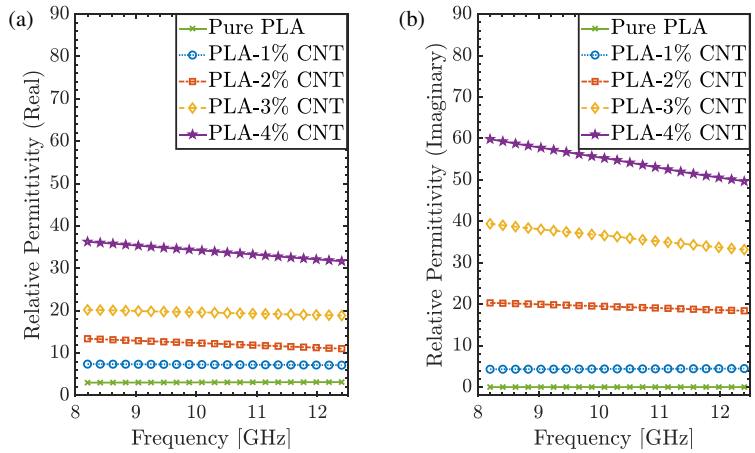

FIGURE 7. (a) Real and (b) imaginary permittivity vs. CNT content for compression-molded samples.

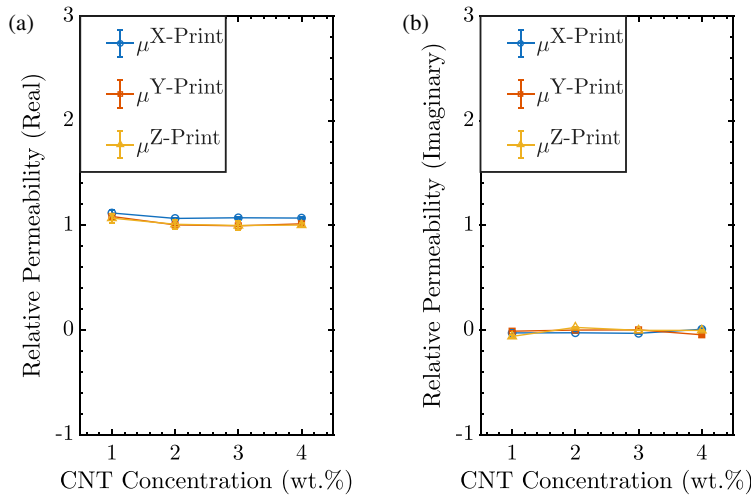

FIGURE 8. (a) Real and (b) imaginary permeability vs. CNT content for different 3D-printed samples. Our model assumes isotropic permeability.

of the dielectric response [40, 41]. In our case, the distinct differences in SE between orientations should not be attributed to structural defects such as air inclusions, as previously discussed, but instead support the hypothesis that CNT alignment governs electromagnetic anisotropy. As such, an anisotropic permittivity tensor can be used to represent the electromagnetic behavior of the printed nanocomposites.

In this study, we characterized the material properties of the samples placed within a rectangular waveguide. The sample was then exposed to TE_{10} mode, in which the electric field was polarized along the z-axis. In this system, the constitutive relations between the electric and magnetic field intensities (E_z, H_x, H_y) and the electric and magnetic flux densities (D_z, B_x, B_y) can be written as follows for the three 3D-printed samples:

$$\text{X-Print:}\ \ D_z = \varepsilon_\perp E_z,\ \ B_x = \mu_\parallel H_x,\ \ B_y = \mu_\perp H_y \quad (2)$$

$$\text{Y-Print:}\ \ D_z = \varepsilon_\perp E_z,\ \ B_x = \mu_\perp H_x,\ \ B_y = \mu_\parallel H_y \quad (3)$$

$$\text{Z-Print:}\ \ D_z = \varepsilon_\parallel E_z,\ \ B_x = \mu_\perp H_x,\ \ B_y = \mu_\perp H_y \quad (4)$$

Because the standard NRW method provides a procedure for extracting the effective isotropic parameters of an unknown medium (i.e., ε_{NRW} and μ_{NRW}), caution must be exercised when applying it to anisotropic samples. We can observe from (4) that when the Z-print sample is placed within the waveguide, only the $\varepsilon_\parallel$ and $\mu_\perp$ components interact with the fields. Therefore, these components can be extracted by setting $\varepsilon_\parallel = \varepsilon_{\text{NRW}}$ and $\mu_\perp = \mu_{\text{NRW}}$. Equations (2) and (3) show that the NRW method cannot be applied to the X-print and Y-print samples if there is anisotropy in the magnetic response (because two different μ components govern the magnetic interaction). However, as shown in the measurements plotted in Figure 3, the SE of the X-print and Y-print samples were nearly identical (within 0.7 dB across all CNT content levels), indicating very little magnetic anisotropy. If we assume that μ is isotropic, we can apply the NRW method to the X-print and Y-print samples to find $\varepsilon_\perp$ and $\mu = \mu_\parallel = \mu_\perp$.

Four samples were fabricated for each of the three orientations (X-print, Y-print, and Z-print) and four CNT weight contents (1%, 2%, 3%, and 4%), resulting in a total of 48 samples (3 orientations $\times$ 4 content levels $\times$ 4 samples each). Figures 8 and 9 plot the real and imaginary extracted permeabilities and permittivities, respectively, averaged over the four samples and averaged over frequency (over the X-band). In addition,

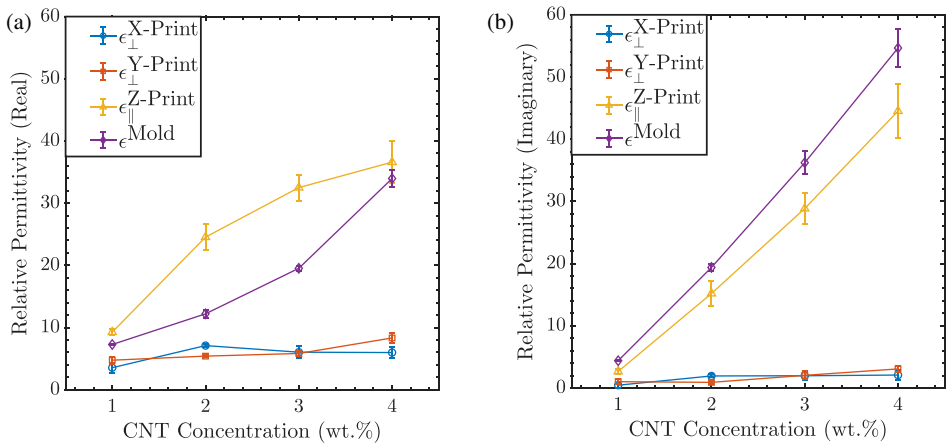

FIGURE 9. (a) Real and (b) imaginary permittivity vs. CNT content for printed samples with three different path orientations and for compression-molded samples.

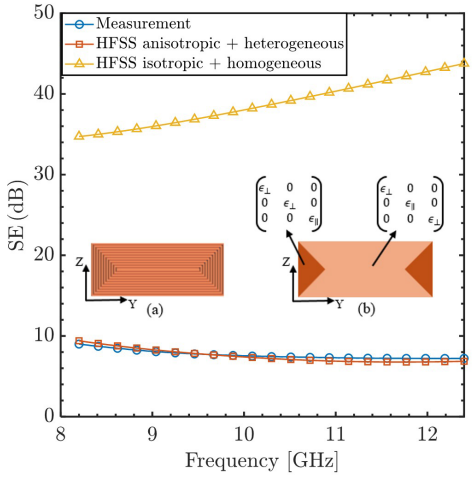

FIGURE 10. Comparison of measured and simulated SE responses of a 3D-printed sample. The simulations were performed using an isotropic and homogenous model with ($\varepsilon = 35 - j55$) and an anisotropic and heterogeneous model specified in the inset diagram. Inset (a) shows the 3D-printed pattern of the structure. Inset (b) shows the simulation model with different anisotropic orientations, distinguished by the light and dark orange regions, using the extracted anisotropic permittivity ($\varepsilon_\perp = 9 - j2.7$, $\varepsilon_\parallel = 35 - j45$).

molded sample data are included in these figures, allowing a direct comparison of the dielectric constants for molded and 3D-printed samples across different CNT loadings and print orientations. Error bars in the figure represent one standard deviation from the mean. For all samples, the variation in the real and imaginary permeabilities across print orientations was within 0.04, with error bars below 0.02. These data confirm the isotropy of the magnetic response, verifying the applicability of the NRW method for characterizing the electric and magnetic responses of nanocomposites. Furthermore, the complex permeability was within 0.1% of $\mu = 1$, which corresponds to a non-magnetic response. In contrast to permeability, the complex permittivity exhibited strong anisotropy. Specifically, $\varepsilon_\parallel$ varied from $9.2 - j2.6$ to $36.5 - j44.5$, and ($\varepsilon_\perp$) varied from $4.7 - j1.1$ to $8.3 - j3.1$ as the CNT content increased from 1% to 4%. The strong dependence of ($\varepsilon_\perp$) on the CNT content is consistent with our model, where the CNTs align with the print orientation as the nanocomposite flows through the printer nozzle.

4.3. Validation of the Anisotropic Model

To emphasize the importance of accurately characterizing the anisotropic electromagnetic properties of 3D-printed nanocomposites, we simulated the shielding effectiveness of a sample printed using concentric paths by employing two different permittivity models. First, we used an isotropic model based on molded sample permittivity ($\varepsilon = 35 - j55$), and in the second, we used the anisotropic permittivity values extracted from our data ($\varepsilon_\perp = 9 - j2.7$ and $\varepsilon_\parallel = 35 - j45$).

We modeled the WR-90 waveguide in HFSS, using its dimensions to replicate the measurement conditions. As demonstrated in Figure 10, there is a difference of more than 24 dB in the SE between the measurement of the 3D-printed sample and the isotropic model in the simulation. However, when considering anisotropic permittivity, the simulation results closely align with the experimental measurements.

These findings highlight the critical need to accurately characterize the anisotropic electromagnetic properties of 3D-printed nanocomposites. They provide valuable insights for future research, underscoring the key role of material anisotropy in the design and simulation of electromagnetic structures using 3D-printed nanocomposites.

5. CONCLUSION

In conclusion, this research highlights the significant impact of 3D printing on the electromagnetic properties of CNT/PLA nanocomposites, particularly in EMI shielding applications. By investigating samples with varying CNT contents (1–4 wt.%) manufactured via compression molding and 3D printing, the study discovers a different anisotropic behavior in the complex dielectric permittivity of the material. Notably, the shielding effectiveness varied by over 20 dB between the printing orientations at the highest CNT loading (4 wt.%), underscoring the critical role of processing conditions.

Through experimental measurements over the X-band frequency range, we developed an anisotropic material model that captures the dependence of dielectric permittivity on CNT orientation. We show that CNT alignment during 3D printing leads to a highly anisotropic permittivity. Specifically, complex permittivity along the printing direction $\varepsilon_{\parallel}$ increases from $9.2 - j2.6$ to $36.5 - j44.5$ as CNT content rises from 1 wt.% to 4 wt.%. In contrast, the perpendicular direction $\varepsilon_{\perp}$ varied from $4.7 - j1.1$ to $8.3 - j3.1$. We also demonstrate the effectiveness of anisotropic models in electromagnetic simulations, showing how they can predict experimental measurements more accurately than isotropic models can.

These findings highlight the impact of the CNT orientation in 3D-printed nanocomposites on the electromagnetic properties of materials. They emphasized the importance of considering anisotropic properties in the design simulations of 3D-printed electromagnetic structures. Additionally, the ability to control electromagnetic properties through print orientation opens new possibilities for tailoring shielding performance in additive manufacturing applications.

ACKNOWLEDGEMENT

This research was financially supported by the Natural Sciences and Engineering Research Council of Canada (NSERC), with funding reference numbers ALLRP 569824-21 and AWD-011907. The authors also acknowledge CMC Microsystems for providing access to the design tools. Additionally, the authors acknowledge Syilx Okanagan Nation for using their traditional, ancestral, and unceded territory, the land on which the research was conducted.

REFERENCES

[1] Wang, H., S. Li, M. Liu, J. Li, and X. Zhou, "Review on shielding mechanism and structural design of electromagnetic interference shielding composites," *Macromolecular Materials and Engineering*, Vol. 306, No. 6, 2100032, 2021.

[2] Yang, Y., M. C. Gupta, J. N. Zalameda, and W. P. Winfree, "Dispersion behaviour, thermal and electrical conductivities of carbon nanotube-polystyrene nanocomposites," *Micro & Nano Letters*, Vol. 3, No. 2, 35–40, 2008.

[3] Murariu, M. and P. Dubois, "PLA composites: From production to properties," *Advanced Drug Delivery Reviews*, Vol. 107, 17–46, 2016.

[4] Kaseem, M., K. Hamad, F. Deri, and Y. G. Ko, "A review on recent researches on polylactic acid/carbon nanotube composites," *Polymer Bulletin*, Vol. 74, No. 7, 2921–2937, 2017.

[5] Spinelli, G., R. Kotsilkova, E. Ivanov, V. Georgiev, C. Naddeo, and V. Romano, "Thermal and dielectric properties of 3D printed parts based on polylactic acid filled with carbon nanostructures," *Macromolecular Symposia*, Vol. 405, No. 1, 2100244, 2022.

[6] Wu, W., T. Liu, D. Zhang, Q. Sun, K. Cao, J. Zha, Y. Lu, B. Wang, X. Cao, Y. Feng, V. A. L. Roy, and R. K. Y. Li, "Significantly improved dielectric properties of polylactide nanocomposites via TiO_2 decorated carbon nanotubes," *Composites Part A: Applied Science and Manufacturing*, Vol. 127, 105650, 2019.

[7] Catarinucci, L., R. Colella, P. Coppola, and L. Tarricone, "Microwave characterisation of polylactic acid for 3D-printed dielectrically controlled substrates," *IET Microwaves, Antennas & Propagation*, Vol. 11, No. 14, 1970–1976, 2017.

[8] Dichtl, C., P. Sippel, and S. Krohns, "Dielectric properties of 3D printed polylactic acid," *Advances in Materials Science and Engineering*, Vol. 2017, No. 1, 6913835, 2017.

[9] Bertašius, P., A. Plyushch, J. Macutkevič, J. Banys, A. Selskis, O. Platnieks, and S. Gaidukovs, "Multilayered composites with carbon nanotubes for electromagnetic shielding application," *Polymers*, Vol. 15, No. 4, 1053, 2023.

[10] Beltrán, F. R., H. Aksas, L. S. Salah, Y. Danlée, and I. Huynen, "Theoretical prediction of electrical conductivity percolation of poly (lactic acid) — Carbon nanotube composites in DC and RF regime," *Materials*, Vol. 16, No. 15, 5356, 2023.

[11] Guan, L.-Z. and L.-C. Tang, "Dispersion and alignment of carbon nanotubes in polymer matrix," in *Handbook of Carbon Nanotubes*, 1–35, Springer, 2021.

[12] Arjmand, M., T. Apperley, M. Okoniewski, and U. Sundararaj, "Comparative study of electromagnetic interference shielding properties of injection molded versus compression molded multi-walled carbon nanotube/polystyrene composites," *Carbon*, Vol. 50, No. 14, 5126–5134, 2012.

[13] Khan, S. U., J. R. Pothnis, and J.-K. Kim, "Effects of carbon nanotube alignment on electrical and mechanical properties of epoxy nanocomposites," *Composites Part A: Applied Science and Manufacturing*, Vol. 49, 26–34, 2013.

[14] Nakamoto, T. and S. Kojima, "Layered thin film micro parts reinforced with aligned short fibers in laser stereolithography by applying magnetic field," *Journal of Advanced Mechanical Design, Systems, and Manufacturing*, Vol. 6, No. 6, 849–858, 2012.

[15] Haslam, M. D. and B. Raeymaekers, "Aligning carbon nanotubes using bulk acoustic waves to reinforce polymer composites," *Composites Part B: Engineering*, Vol. 60, 91–97, 2014.

[16] Li, J., T. Guan, Z. Zhang, Y.-T. Fu, F.-L. Guo, P. Huang, Z. Li, Y.-Q. Li, and S.-Y. Fu, "Orientation of discontinuous fillers in polymer composites: Modelling, characterization, control and applications," *Progress in Materials Science*, Vol. 148, 101360, 2025.

[17] Oussai, A., Z. Bártfai, and L. Kátai, "Development of 3D printing raw materials from plastic waste. A case study on recycled polyethylene terephthalate," *Applied Sciences*, Vol. 11, No. 16, 7338, 2021.

[18] Alarifi, I. M., "Revolutionising fabrication advances and applications of 3D printing with composite materials: A review," *Virtual and Physical Prototyping*, Vol. 19, No. 1, e2390504, 2024.

[19] Zohdi, N. and R. Yang, "Material anisotropy in additively manufactured polymers and polymer composites: A review," *Polymers*, Vol. 13, No. 19, 3368, 2021.

[20] Truman, L., E. Whitwam, B. B. Nelson-Cheeseman, and L. J. Koerner, "Conductive 3D printing: Resistivity dependence upon infill pattern and application to EMI shielding," *Journal of Materials Science: Materials in Electronics*, Vol. 31, No. 17, 14 108–14 117, 2020.

[21] Wu, T., X. Huan, H. Zhang, L. Wu, G. Sui, and X. Yang, "The orientation and inhomogeneous distribution of carbon nanofibers and distinctive internal structure in polymer composites induced by 3D-printing enabling electromagnetic shielding regulation," *Journal of Colloid and Interface Science*, Vol. 638, 392–402, 2023.

[22] Harmon, A., W. Zhang, and V. Khilkevich, "On the permittivity of XT-CF20," in *2023 IEEE Symposium on Electromagnetic Compatibility & Signal/Power Integrity (EMC+SIPI)*, 390–394, Grand Rapids, MI, USA, 2023.

[23] Harmon, A., V. Khilkevich, and K. M. Donnell, "High permittivity anisotropic 3D printed material," in *2022 IEEE International*

Symposium on Electromagnetic Compatibility & Signal/Power Integrity (EMCSI), 1–6, Spokane, WA, USA, 2022.

[24] Mahaut, V., T. Dubois, A. Gracia, G. Foyer, and W. Maia, "Assessment of the shielding efficiency of FDM-produced continuous carbon fiber composites," in *2024 25th International Conference on Thermal, Mechanical and Multi-Physics Simulation and Experiments in Microelectronics and Microsystems (EuroSimE)*, 1–6, Catania, Italy, 2024.

[25] Compton, B. G. and J. A. Lewis, "3D-printing of lightweight cellular composites," *Advanced Materials*, Vol. 26, No. 34, 5930–5935, 2014.

[26] Isari, A. A., A. Ghaffarkhah, S. A. Hashemi, S. Wuttke, and M. Arjmand, "Structural design for EMI shielding: From underlying mechanisms to common pitfalls," *Advanced Materials*, Vol. 36, No. 24, 2310683, 2024.

[27] Kazani, I., G. De Mey, C. Hertleer, J. Banaszczyk, A. Schwarz, G. Guxho, and L. Van Langenhove, "About the collinear four-point probe technique's inability to measure the resistivity of anisotropic electroconductive fabrics," *Textile Research Journal*, Vol. 83, No. 15, 1587–1593, 2013.

[28] Barnes, H. A., "A review of the rheology of filled viscoelastic systems," *Rheology Reviews*, 1–36, 2003.

[29] Es-Said, O. S., J. Foyos, R. Noorani, M. Mendelson, R. Marloth, and B. A. Pregger, "Effect of layer orientation on mechanical properties of rapid prototyped samples," *Materials and Manufacturing Processes*, Vol. 15, No. 1, 107–122, 2000.

[30] Mazzanti, V., L. Malagutti, and F. Mollica, "FDM 3D printing of polymers containing natural fillers: A review of their mechanical properties," *Polymers*, Vol. 11, No. 7, 1094, 2019.

[31] Abbasi, S., P. J. Carreau, and A. Derdouri, "Flow induced orientation of multiwalled carbon nanotubes in polycarbonate nanocomposites: Rheology, conductivity and mechanical properties," *Polymer*, Vol. 51, No. 4, 922–935, 2010.

[32] Verma, P., T. Bansala, S. S. Chauhan, D. Kumar, S. Deveci, and S. Kumar, "Electromagnetic interference shielding performance of carbon nanostructure reinforced, 3D printed polymer composites," *Journal of Materials Science*, Vol. 56, No. 20, 11 769–11 788, 2021.

[33] Nicolson, A. M. and G. F. Ross, "Measurement of the intrinsic properties of materials by time-domain techniques," *IEEE Transactions on Instrumentation and Measurement*, Vol. 19, No. 4, 377–382, 1970.

[34] Costa, F., M. Borgese, M. Degiorgi, and A. Monorchio, "Electromagnetic characterisation of materials by using transmission/reflection (T/R) devices," *Electronics*, Vol. 6, No. 4, 95, 2017.

[35] Chen, H., J. Zhang, Y. Wang, W. Che, Z. Huang, Y. Qiao, J. Luo, and Q. Xue, "An improved NRW method for thin material characterization using dielectric filled waveguide and numerical compensation," *IEEE Transactions on Instrumentation and Measurement*, Vol. 71, 1–9, 2022.

[36] Jiang, M.-J., Z.-M. Dang, M. Bozlar, F. Miomandre, and J. Bai, "Broad-frequency dielectric behaviors in multiwalled carbon nanotube/rubber nanocomposites," *Journal of Applied Physics*, Vol. 106, No. 8, 084902, 2009.

[37] Nelson, J. K. and J. C. Fothergill, "Internal charge behaviour of nanocomposites," *Nanotechnology*, Vol. 15, No. 5, 586, 2004.

[38] Xu, N., P. P. Yong, and Z. Wang, "Large dielectric constant and Maxwell-Wagner effects in $BaTiO_3$/Cu composites," *Journal of the American Ceramic Society*, Vol. 95, No. 3, 999–1003, 2012.

[39] Cao, W.-Q., Q. Zheng, L. Li, C.-B. Cao, and M.-S. Cao, "Dielectric genetic tailoring strategy dominating $MoSe_2$@rGO assembled architecture with electromagnetic functions," *Journal of Advanced Ceramics*, Vol. 13, No. 9, 1461–1472, 2024.

[40] Mikki, S. M. and A. A. Kishk, "Mean-field electrodynamic theory of aligned carbon nanotube composites," *IEEE Transactions on Antennas and Propagation*, Vol. 57, No. 5, 1412–1419, 2009.

[41] Nefedov, I. S. and S. A. Tretyakov, "Effective medium model for two-dimensional periodic arrays of carbon nanotubes," *Photonics and Nanostructures — Fundamentals and Applications*, Vol. 9, No. 4, 374–380, 2011.